Spectroscopic Investigation of a Ruthenium Tris-Diimine Complex Featuring a Bioinspired Alloxazine Ligand

Nina Hagmeyer, Alexander Schwab, Nabil Mroweh, Caitilin Mcmanus, Maneesha Varghese, Jean-Marie Mouesca, Serge Gambarelli, Stephan Kupfer, Murielle Chavarot-Kerlidou, Benjamin Dietzek-Ivanšić

ChemPhotoChem

Research Article
doi.org/10.1002/cptc.202400175

Chemistry Europe
European Chemical Societies Publishing

www.chemphotochem.org

Spectroscopic Investigation of a Ruthenium Tris-Diimine Complex Featuring a Bioinspired Alloxazine Ligand

Nina Hagmeyer,[a, b] Alexander Schwab,[a] Nabil Mroweh,[c] Caitilin McManus,[c] Maneesha Varghese,[d] Jean-Marie Mouesca,[d] Serge Gambarelli,[d] Stephan Kupfer,*[a] Murielle Chavarot-Kerlidou,*[c] and Benjamin Dietzek-Ivanšić*[a, b]

Molecular charge accumulating systems that act as both, photosensitizer and electron storage unit, are of interest in the context of multielectron redox processes, e.g. in solar fuel production. To this end, the photophysical properties of **RuL1**, a ruthenium tris-diimine complex with an alloxazine-based ligand as bioinspired structural motif, were investigated. The study includes absorption, emission, resonance Raman and transient absorption spectroscopy in combination with quantum chemical simulations to determine the light-driven reactivity of the complex. Moreover, spectroelectrochemistry was employed for an in-depth characterization of the optical properties of the reduced complex. Finally, a photolysis experiment using triethanolamine as electron source, in conjunction with redox titrations, demonstrated that visible light irradiation triggers the formation of the doubly-reduced singly-protonated derivative of **RuL1**, where both redox equivalents are stored on the alloxazine-based ligand.

Introduction

Designing molecular assemblies combining light harvesting and multiple charge storage properties has recently attracted a growing interest in the field of artificial photosynthesis.[1–4] Charge accumulation is indeed a mandatory step in multielectron fuel-forming reactions such as water splitting or CO_2 reduction driven by light. Several successive photoinduced charge separation processes are necessary to generate the required redox equivalents, and the ability to temporarily store these charges on well-defined sites is essential. Subsequently, these redox equivalents may be delivered to a catalytic center. This approach is foreseen as an efficient strategy to drastically reduce charge recombination and therefore increase photocatalytic efficiency. Since the initial study from Wasielewski in 1992, various molecular systems have been reported to show light-driven accumulation of multiple reducing equivalents.[1–5] Among these, mononuclear Ru(II) tris-diimine photosensitizers featuring a single peripheral ligand as electron storage reservoir[6–12] are particularly suitable for subsequent coupling with a catalyst. In nature, specific enzymes and cofactors are also key players to decouple dark reactions (i.e. catalysis) from light reactions (i.e. light harvesting and photoinduced charge separation) in the photosynthetic process. Typically, the ferredoxin-$NADP^+$-reductase (FNR) mediates electron transfer from the single-electron carrier ferredoxin to the two-electron carrier NADPH thanks to its flavin cofactor: the flavin-adenine-dinucleotide (FAD) is reduced twice during this process. The reductions are coupled to proton transfer events to avoid excessive charge build-up and to stabilize intermediate species. Consequently, artificial photosynthesis takes inspiration from such natural electron relays. Flavins are widely studied as photoactive components in photocatalytic redox reactions[13–15] and coupling the favorable (optical) characteristics of Ru-polypyridyl complexes (high chemical stability, long-lived excited states) with the $2e^-/2H^+$ redox chemistry of flavins renders them suitable candidates for light-driven redox chemistry.[16] There are some reports on ruthenium complexes containing flavin motifs,[16–20] e.g. by Miyazaki et al. who showed the effect of non-covalent interactions on the physical properties of their complexes[17] and by Black et al. who reported the complex **RuL1** (see Figure 1) featuring an alloxazine moiety.[18]

[a] N. Hagmeyer, A. Schwab, Dr. S. Kupfer, Prof. Dr. B. Dietzek-Ivanšić
Faculty of Chemistry and Earth Science
Institute of Physical Chemistry, Friedrich Schiller University
Lessingstraße 4, 07743 Jena, Germany
E-mail: benjamin.dietzek@uni-jena.de
stephan.kupfer@uni-jena.de

[b] N. Hagmeyer, Prof. Dr. B. Dietzek-Ivanšić
Department of Functional Interfaces
Leibniz Institute of Photonic Technology
Albert-Einstein-Straße 9, 07745 Jena, Germany

[c] Dr. N. Mroweh, Dr. C. McManus, Dr. M. Chavarot-Kerlidou
Univ. Grenoble Alpes, CNRS, CEA, IRIG
Laboratoire de Chimie et Biologie des Métaux
17 rue des Martyrs, F-38054 Grenoble, Cedex, France
E-mail: murielle.chavarot-kerlidou@cea.fr

[d] Dr. M. Varghese, Dr. J.-M. Mouesca, Dr. S. Gambarelli
Univ. Grenoble Alpes, CNRS, CEA, IRIG
SyMMES
17 rue des Martyrs, F-38054 Grenoble, Cedex, France

Supporting information for this article is available on the WWW under https://doi.org/10.1002/cptc.202400175

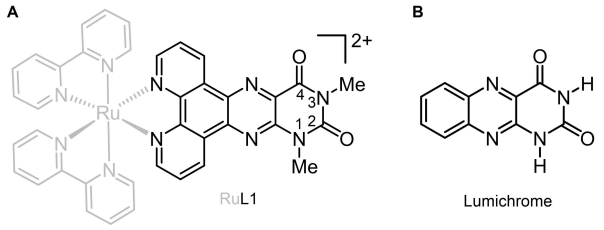

Figure 1. Chemical structures of the bioinspired ruthenium complex **RuL1** investigated in this work (A) and of lumichrome (B), the structural motif incorporated in **RuL1**.

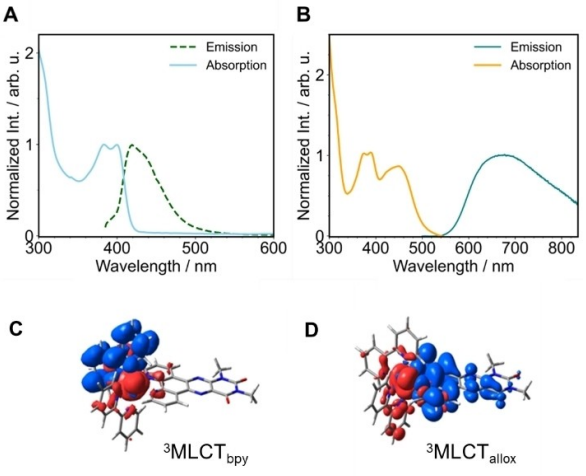

Figure 2. UV–Vis absorption and emission spectra of **L1** in DMSO (A) and **RuL1** in CH_3CN (B). Relaxed $^3MLCT_{bpy}$ (C) and $^3MLCT_{allox}$ (D) species which are potentially associated with the emission. Electronic characters are visualized by charge density difference plots; charge transfer occurs from red to blue.

However, the potential of such Ru-polypyridyl-flavin complexes for light-driven multiple charge accumulation has not yet been explored.

The studies performed by Black et al. include cyclic voltammetry of **RuL1** in acetonitrile (CH_3CN), dimethyl sulfoxide (DMSO) and aqueous buffer solution, in which it undergoes a reversible $2e^-/2H^+$ electrochemical process on the alloxazine ligand.[18] Based on these data, we decided to investigate the photophysical and photochemical properties of **RuL1** in more detail and assess its suitability for light-driven charge accumulation and electron storage. To this end, steady-state absorption measurements of the neutral species and, with the help of spectroelectrochemistry (SEC), the singly reduced species were conducted. Quantum-chemical calculations as well as resonance Raman (rR) spectroscopy were employed to unravel the optical transitions observed in the absorption measurements. Redox titrations of **RuL1** and density functional theory (DFT) simulations yielded a set of reference data for the identification of various redox (and pH-dependent) intermediates and photoproducts playing a role in the charge accumulation process. The photoreactivity was assessed by transient absorption (TA) spectroscopy, which, in combination with time-dependent DFT (TDDFT) simulations, elucidates the excited-state dynamics and characterizes the long-lived excited state which will take part in the light-driven redox reaction. Finally, a photolysis experiment in the presence of triethanolamine (TEOA) as electron donor allowed us to assess the ability of **RuL1** to accumulate redox equivalents.

Results and Discussion

Spectroscopic Characterization of RuL1

The UV–Vis absorption spectrum of **L1** dissolved in DMSO (see Figure 2A) was measured in addition to **RuL1** for comparison and exhibits a band at 260 nm with a shoulder at 300 nm as well as a double band feature with maxima at 384 and 400 nm. The latter are attributed to π–π* transitions of the alloxazine core.[6,7,8] The complex **RuL1** features absorption peaks at 288, 378 and 392 nm in DMSO (see Figure S1) which are slightly blueshifted to 280, 374 and 389 nm in acetonitrile (see Figure 2B). These bands are attributed to intra-ligand charge transfer (ILCT) and π–π* transitions (within the alloxazine system, as well as within the bipyridine (bpy) systems) as predicted by TDDFT simulations (Figure S2, Table S1 and S2).

Additionally, the characteristic metal-to-ligand charge transfer (MLCT) transitions are observed between 400–510 nm. The underlying transitions are associated with the S_4 (484 nm), S_5 (483 nm), S_{10} (433 nm) and S_{12} (425 nm) MLCT states, which involve the entire ligand sphere, as well as the S_{11} state (429 nm), which features excitation solely towards the bpy moiety (see supporting information for more detailed assignments of transitions). The electronic characters of these states and transitions will be further discussed within the context of the rR experiments. The ligand itself shows an emission band at 419 nm whereas the emission spectrum of the complex is found at longer wavelengths with a maximum at 675 nm. The spectral shape is independent of the excitation wavelength and the excitation spectra reflect the absorption spectrum of the complex (see Figure S3), as expected. Based on studies of related Ru complexes,[21] e.g. $[Ru(bpy)_2(dppz)]^{2+}$ (Ru(dppz)) the emission originates from radiative decay of a ^{3}MLCT state. It should be noted that the emission maximum of **RuL1** is significantly redshifted compared to Ru(dppz) implying that the emissive state is lower in energy.[22] The fact that the emission wavelength matches neither the one found for Ru(dppz) nor $Ru(bpy)_3$ indicates that the emissive state involves the alloxazine unit of the ligand (see Figure 2D). We hypothesize that the additional electron-withdrawing groups, i.e. nitrogen and carbonyl groups in position 1 to 4 affect the energy gap between the singlet ground-state and the lowest triplet state and hence the luminescence properties. Optimization of the lowest energy triplet state geometry of **RuL1** from the Franck-Condon point by the means of DFT initially lead to a ^{3}MLCT state with a spin density distributed over the bpy co-ligands and the Ru-center – i.e., a $^3MLCT_{bpy}$ species with a predicted emission wavelength of 649 nm (see Figure 2C). This value slightly differs from experimental results by +0.07 eV. There-

fore, further (low-lying) triplet states were considered and optimized via TDDFT and the external optimizer *pysisyphus*.[23] This revealed that the excited state T_3 – of $^3MLCT_{allox}$ character – becomes the triplet ground state in its equilibrated structure. This $^3MLCT_{allox}$ state is quasi isoenergetic (+0.03 eV) in comparison to the initially found $^3MLCT_{bpy}$ and should therefore be easily populated at ambient temperature. Moreover, the calculated emission wavelength of 678 nm obtained for the $^3MLCT_{allox}$ species is in excellent agreement with the experimental findings (675 nm; deviation of merely −0.01 eV). Thus, we associate the emission of **RuL1** with a ^{3}MLCT species that involves the excited electron being localized on the alloxazine-based ligand. Noteworthy, T_2 is also of $^3MLCT_{bpy}$ character but involves the second bpy ligand; this state will not be discussed further in the following.

Resonance Raman spectroscopy complements the UV–Vis absorption experiments and the theoretical analysis of the absorption features of the complex.[24] The spectra were recorded upon excitation at 405 and 473 nm (Figure 3). The spectra are similar to the parent complex Ru(dppz) and consist of vibrational modes of both, the bpy ligands as well as the dppz-like extended alloxazine ligand. Consequently, MLCT transitions involving the entire ligand sphere contribute to both spectral regions, i.e., excitation at 405 nm as well as 473 nm. Nonetheless, the spectra reveal some excitation wavelength-dependent differences. In particular, one Raman band which is only present upon 405-nm excitation is found at 1237 cm^{-1}. This band is not present in any of the spectra of Ru(dppz) and can, thus, be attributed to the alloxazine/uracil moiety. We assume that, apart from the MLCT transitions, a transition which is localized on the alloxazine part of the ligand contributes to the absorption in the spectral region around 405 nm. Theoretical calculations confirm the presence of bright MLCT transitions into S_{10}, S_{11} and S_{12} which are in resonance with the 405-nm excitation. These states are associated with an electron density shift from the Ru(II) ion towards the bpy co-ligands ($^1MLCT_{bpy}$) as well as the alloxazine ligand. Moreover, the 405-nm excitation is partially in resonance with an optical transition to the ILCT state S_{16} at 365 nm. Based on the simulated rR intensity pattern, this ILCT transition is associated with the enhancement of the measured band at 1237 cm^{-1} of **RuL1** and can be assigned to a vibrational normal mode of the alloxazine moiety, i.e. mode 149 with a high relative intensity of 0.24 (see calculated rR spectrum Figure S4 and Table S3). Optical excitation at 473 nm also populates the states S_{10}, S_{11} and S_{12} but additionally leads to population of the states S_4 and S_5 which, again, have mixed bpy and **L1** character. Thereby, the theoretical calculations support the assignment of the experimental data in that the MLCT transition are similar to the parent complex Ru(dppz), i.e. the charge is distributed onto all ligands. In summary, upon 405-nm excitation, an optical transition localized on the alloxazine ligand is induced besides the MLCT transitions. This should be kept in mind as the excitation of an additional, ligand-based transition at 405 nm could potentially lead to a modified relaxation path compared to the pure MLCT excitation. Therefore, a different photoreactivity than for excitation in the MLCT region might be observed.

Having characterized the Franck-Condon photophysics by UV–Vis and rR spectroscopy in combination with TDDFT simulations, the following section aims at elucidating the excited-state dynamics and relaxation pathways of **L1** and **RuL1**. These determine their photoreactivity and, hence, their charge accumulation ability. Transient absorption spectroscopy with a sub-100 fs time resolution was employed and will be discussed in the following. Figure 4A–C displays the TA data of **L1** upon excitation at 405 nm. At early delay times, they show an excited-state absorption (ESA) band between 400–450 nm and a broad ESA above 500 nm. This shape resembles the triplet state spectra of lumichrome derivatives which consist of a peak around 370 nm and a broad, less intense band above 400 nm.[25] However, the triplet state spectra of known lumichrome derivatives are blueshifted to what is observed for **L1**. At later delay times, the spectral shape changes to an ESA spanning from 380–700 nm, which has a maximum at 480 nm and two shoulders at 415 and 560 nm. These two features are best seen from the species-associated spectrum (SAS) of the long-lived species (Figure 4C, inset). Kinetic analysis reveals three species described by the characteristic time constants τ_1 = 5.7 ps and τ_2 = 65 ps and τ_3 which lies in the ns range, i.e., beyond the experimentally accessible dynamic range. Based on literature on solvent reorganization as well as on lumichrome

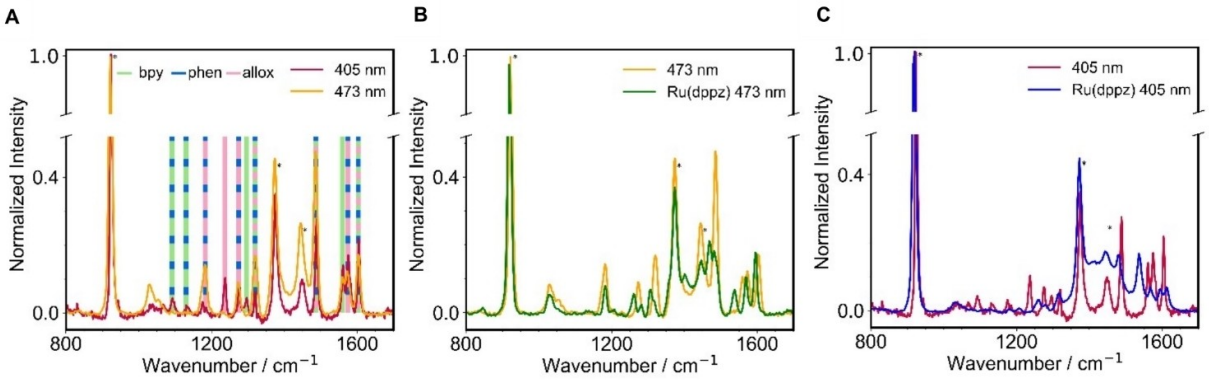

Figure 3. Resonance Raman (rR) spectra of **RuL1** in CH_3CN after excitation at 405 and 473 nm (A) and comparison with the spectra of Ru(dppz) after excitation at 473 nm (B) and 405 nm (C). The spectra were normalized to the solvent peak at 920 cm^{-1}. Solvent peaks are marked by an asterix.

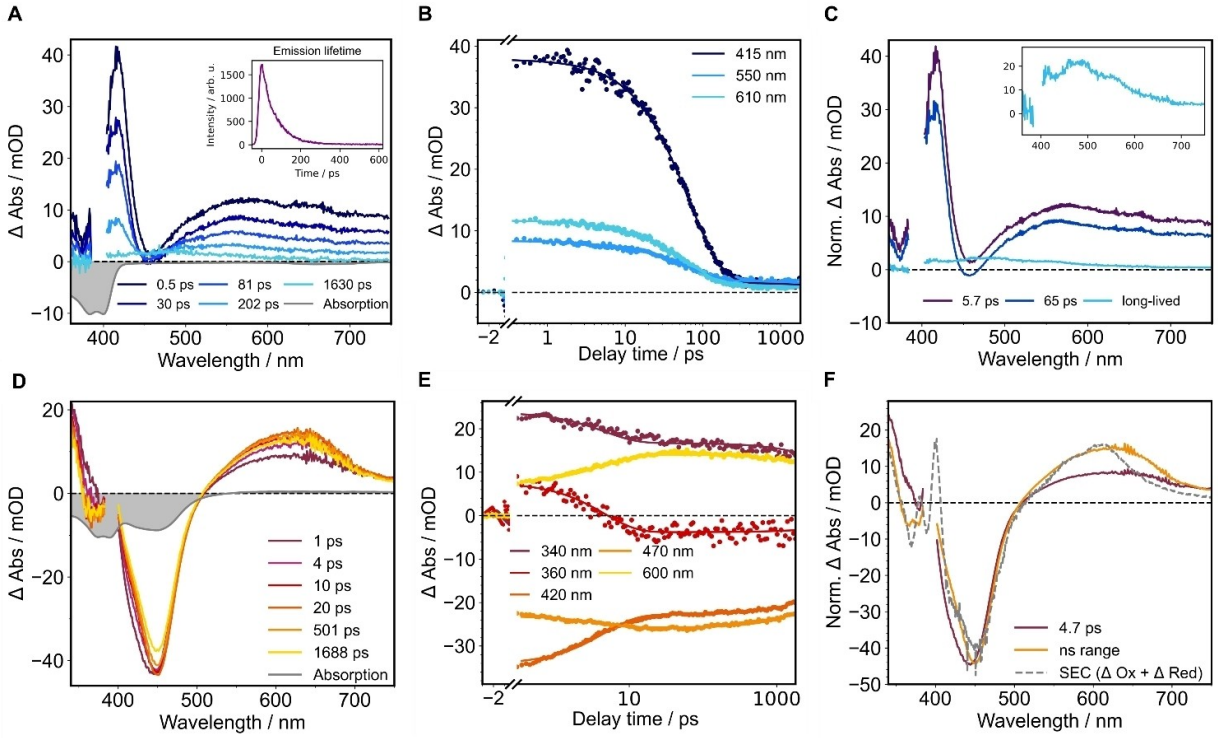

Figure 4. (A) Transient absorption spectra of **L1** in DMSO at different delay times after excitation at 405 nm. The inset in panel A shows the kinetic trace of the time-resolved emission measured via streak camera. (B) Kinetic traces of the transient absorption measurements at selected wavelengths and (C) corresponding species-associated spectra (SAS) obtained from global analysis. The inset in panel C shows the SAS associated with the long-lived species. (D) Transient absorption spectra of **RuL1** in CH_3CN at different delay times after excitation at 405 nm, (E) kinetic traces at selected wavelengths and (F) SAS obtained by applying a global fit to the data. The grey line in panel F represents the simulated MLCT spectrum obtained by the sum of the difference spectra of the singly oxidized and singly reduced complex.

and dppz excited-state dynamics,[26–28] the first species is attributed to an S_N state which, subsequently, relaxes to the lowest excited singlet state. Apart from internal conversion and solvent reorganization, this process likely comprises vibrational cooling which is reported to take place on a similar timescale for an alloxazine analogue.[27] The second characteristic time component is comparable to the emission lifetime of the ligand, which was determined to be ~80 ps via streak camera (see Figure 4A inset). Hence, τ_2 is assigned to the lifetime of the S_1 state. The resemblance of the singlet spectrum of **L1** with the triplet state of lumichrome analogues[25] could be explained by a similar geometry and electronic structure of the two spin states so that the general spectral shape is maintained. As described above, the triplet state spectra of lumichrome derivatives reported in literature consist of a peak around 370 nm and a band above 400 nm. The apparent blueshift of these spectra compared to the transient absorption spectra shown here might be due to the lower energy of the triplet state which translates to a higher energy gap between this triplet state and the state which is populated upon interaction with the probe pulse. The similarity to the lumichrome spectrum also indicates that the S_1 state of **L1** is mostly associated with the alloxazine-like part of the ligand. The spectral shape at longer delay times (and the SAS of the long-lived species) resembles the spectral features of the previously reported triplet state of dppz.[28] Its spectrum spans from ~370–700 nm and consists of peaks at 390 and 460 nm and a broad shoulder around 580 nm. Moreover, Zhang et al. reported a characteristic time constant of 46 ps for the intersystem crossing (ISC) in dppz[28] which matches the timescale we observe for the formation of the long-lived state of **L1** (described by τ_2). Therefore, this state, which is associated to τ_3, is assigned to a more dppz-like triplet state. ISC from the triplet state to the electronic ground-state occurs on a timescale beyond the ones accessible in our experiment. The corresponding relaxation pathway is illustrated in Figure 5A. The TA spectra of **RuL1** in CH_3CN are shown in Figure 4D–F. Additionally, measurements in DMSO were performed to ensure comparability to the results obtained for the ligand. These are shown and discussed in the supporting information (Figure S5). Below 400 nm a super-

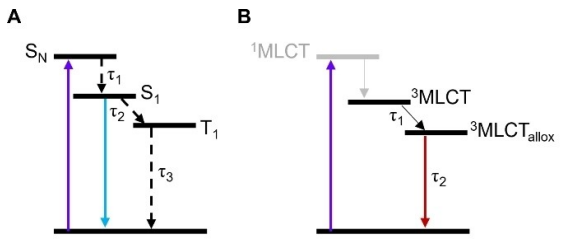

Figure 5. Jablonski diagram for the ligand **L1** (A) and the complex **RuL1** (B) upon excitation at 405 nm.

position of ground state bleach (GSB) and ESA from ligand-centered transitions is observed. The region from 410–510 nm is dominated by GSB whereas an ESA band is visible above 520 nm. The overall shape of the spectra does not change drastically over time. Nonetheless, a decrease of the feature below 400 nm can be observed within the first 10 ps and the contribution of the GSB between 360–400 nm becomes more pronounced resulting in a negative signal after ~3 ps. Additionally, the signal in the 410–510 nm-region narrows, especially on the blue edge. Global analysis of the data yields two characteristic first-order time constants, $\tau_1 = 4.7$ ps while τ_2 lies in the ns range. It should be noted that ISC of ruthenium polypyridyl complexes typically proceeds faster than the time resolution achieved with our experimental setup[29] so that the observed processes are ascribed to a ^{3}MLCT species. The spectral differences between the first and second species obtained from global analysis manifest themselves in an increase of the signal between 400–450 nm and above 500 nm as well as a decrease of the ESA between 340–380 nm, especially around 360 nm (see Figure 4F). These spectral changes are interpreted as reduction of the alloxazine unit of the ligand, i.e., reflecting interligand and intraligand charge transfer from the bpy[30] ligands and the phen unit (^{3}MLCT) to the alloxazine part of extended ligand ($MLCT_{allox}$). This is inferred from the absence of recovery of ground-state absorption and the decrease of the peak at 360 nm, which matches the signal[31,32] of phen$^{-\bullet}$ while the reduced alloxazine shows an absorption peak around 340 nm (Figure S6). Moreover, the increase of the signal between 400–450 nm, which leads to narrowing of the GSB feature, is in the same spectral range as the spectral maximum of the alloxazine anion radical (Figure S6) corroborating that part of the electron density is shifted to this part of the ligand. Additionally, the MLCT spectrum approximated[33] by a linear combination of the spectra of the reduced (see Figure 6) and oxidized complex (see Figure S7) reproduces the spectral features found at long delay times which are represented by the ns-SAS (see Figure 4F).

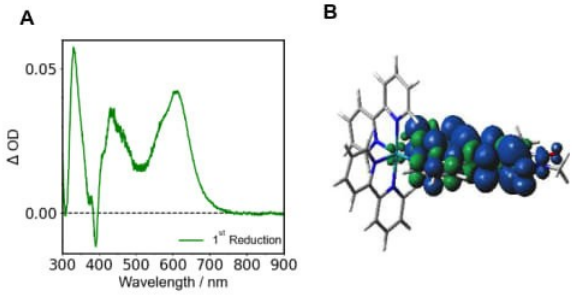

Figure 6. UV–Vis difference absorption spectra of **RuL1** in CH_3CN (A) recorded at an applied potential corresponding to the first reduction potential. The electrolytes contained 0.1 M $TBAPF_6$ (scan rate 100 mV·s^{-1}, glassy carbon working electrode, Pt counter electrode and Ag/AgCl pseudo-reference electrode). (B) Spin density which shows the localization of the additional electron added within the doublet species of singly reduced **RuL1**.

Hence, this component describes the lifetime of the $^3MLCT_{allox}$ (see Figure 5B).

The TA spectra were also simulated using TDDFT by calculating the spin and dipole-allowed triplet-triplet excitations to assess the ESA for the two previously discussed triplet species, namely $^3MLCT_{bpy}$ and $^3MLCT_{allox}$ (see Figure S8, Table S4 and S5 as well as Figure S9, Table S6 and S7). Both simulated spectra of the species, $^3MLCT_{bpy}$ and $^3MLCT_{allox}$, are in good agreement with the experimental data. As shown by TDDFT, the two simulated TA spectra of the discussed ^{3}MLCT states differ mainly in the predicted ESA within the spectral window between 500 and 600 nm i.e., the states T_{16} (561 nm, $LMCT_{bpy}$) and T_{20} (514 nm, $LMCT_{allox}$), which were only accessible if the alloxazine moiety was populated in the triplet ground state. Thus, an unambiguous assignment of the excited state processes based on the simulated spectra of the key excited states – $^3MLCT_{bpy}$ vs. $^3MLCT_{allox}$ – is unfortunately impossible in the present case. The phosphorescence of **RuL1** is expected to originate from the long-lived charge-separated state ($MLCT_{allox}$) observed in the TA measurements. Therefore, emission lifetime measurements on the nanosecond scale were performed to determine its lifetime. A global fit of the decay curves (Figure S10) yields a monoexponential decay of the phosphorescence and a lifetime of around 21 ns which is three orders of magnitude greater than the fluorescence lifetime of the pure ligand. With this lifetime and the fact that a charge-separated state is observed, two requirements for intermolecular reactivity are fulfilled which makes **RuL1** a promising candidate for photochemical reactions and light-driven charge accumulation.

Spectroscopic Characterization of the Singly Reduced Species

In the context of photoinduced molecular charge accumulation, the singly reduced species represents a key intermediate. To gain more insight into its properties, this species was (electro)chemically generated and investigated by UV–Vis absorption and rR spectroscopy, supported by DFT and TDDFT calculations. The singly reduced complex shows a new absorption band at 610 nm, enhanced absorption in the MLCT region of the neutral complex, especially at 430 nm, and reduced absorption around 390 nm (see Figure 6). The latter represents the region of the π–π* transitions of the alloxazine core.[18,34] These spectral changes point towards localization of the additional charge on the extended ligand as reduced alloxazine shows an absorption feature between 400–550 nm (Figure S6). This assignment is further corroborated by the fact that the reduced ligand **L1** also shows a band in the red region similar to the band observed at 610 nm in the complex (Figure S6).

The described charge distribution upon one-electron reduction is also supported by theoretical calculations, which reveal that the first reduction is alloxazine-centered as shown by the entire spin density in Figure 6B. Subsequent TDDFT calculations of the singly reduced species helped in shedding more light on the nature of the characteristic bands of the UV–Vis spectrum of **RuL1** i.e., the observed band at 610 nm could be attributed

to the D_9 doublet excited state, which is an ILCT within the alloxazine ligand (more detailed information can be found in the supporting information Table S8 and S9). Resonance Raman spectroscopy of the reduced complex was employed to further corroborate this interpretation experimentally as the method allows to draw conclusions about the position of the additional charge, e.g. by determining the moieties linked to the spectral changes. The corresponding results (see Figure 7) are discussed in the next section. Resonance Raman measurements were performed on the chemically reduced complex where cobaltocene served as reducing agent. Excitation wavelengths of 473 and 643 nm were chosen. For 473-nm excitation, an additional peak evolves at 1240 cm^{-1} and instead of a double peak at 1560–1580 cm^{-1}, a single peak at 1560 cm^{-1} is found whereas the remaining peak positions are similar to the neutral complex. Nonetheless, the relative intensity between the peaks is altered. All peaks which can solely be attributed to the alloxazine ligand decrease in intensity by ~30–40% relative to the other peaks. More specifically, these are found at 1446, 1575 and around 1370 cm^{-1}. This suggests that optical excitation of the MLCT band of the reduced complex leads to charge density being preferentially shifted from the Ru(II) center to the bpy. The result agrees with the additional negative charge being mostly localized on the alloxazine ligand which, consequently, accepts less charge of the Ru center upon excitation of the MLCT transition. Furthermore, the TDDFT results of the singly-reduced doublet species suggest that the doublet excited states D_{24} (448 nm) and D_{26} (432 nm), which are both of $^2MLCT_{bpy}$ character, could possibly be excited in the 473 nm experiment (Figure S11). In order to determine the origin of the absorption band at 610 nm, which evolves upon reduction of the complex, rR spectra upon excitation at 643 nm were recorded. Vibrational modes which are visible upon excitation at 643 nm are associated with the absorption band which is only present in the reduced species. This information can further help identifying the electronic changes which follow reduction of the complex. Apart from the solvent bands, the rR spectra show peaks at 1445, 1507 and 1592 cm^{-1} all of which can be attributed to the alloxazine-like ligand. This confirms the assignment of the new absorption band to a ligand-centered optical transition and supports the hypothesis that the additional negative charge is rather localized on the alloxazine-like structure than on the bpy ligands.

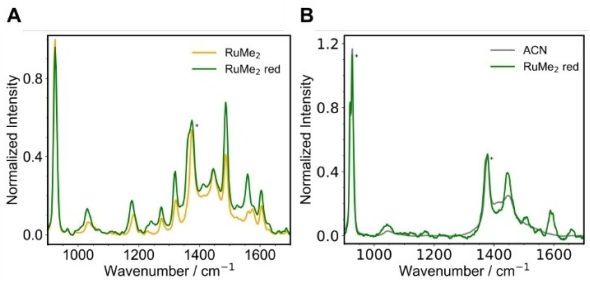

Figure 7. Resonance Raman spectra of **RuL1** in CH_3CN reduced with cobaltocene upon excitation at 473 nm (A) and 643 nm (B).

Investigation of Multiple Charge Accumulation: Light-Driven versus Chemical Reduction

As described above, the first reduction of **RuL1** takes place on the alloxazine-based ligand, associated with the population of its lowest lying π^*_{allox} orbital. This process does not affect the position of the broad MLCT absorption between 400 and 500 nm of the ruthenium tris-diimine complex but an increase in absorbance is observed. It was therefore tempting to investigate **RuL1**'s light-driven reactivity, and more specifically its ability to achieve photoinduced accumulation of multiple reducing equivalents. A photolysis experiment was performed under anaerobic conditions in CH_3CN in the presence of triethanolamine (TEOA) as sacrificial electron donor and was monitored by UV–Vis absorption spectroscopy (Figure 8A). Upon visible light irradiation, very fast changes of the initial absorption of **RuL1** are observed and the formation of the singly-reduced species is detected within the first 30 s (Figure 8B); this reactivity is in agreement with reductive quenching of the excited state of **RuL1** by TEOA. However, this species is not the final product of the photochemical reaction, as the absorption of the solution continues to evolve under irradiation. Particularly noteworthy are the decrease of the absorption bands at 610 nm, characteristic of the singly-reduced species, and at 375 nm, attributed to a π–π^* transition of the alloxazine ligand; the described changes are accompanied by a further increase in the MLCT absorption at 450 nm. In order to identify the photoproduct formed during the photolysis, we decided to investigate the reactivity of the singly-reduced complex in the presence of TFA as proton source. Indeed, it is well-known that protons released from the decomposition of the TEOA radical cation[35] (generated in the photolysis experiment after reductive quenching of the excited state of **RuL1** by TEOA) can protonate the photogenerated species.[8,11,12] Figure 8E shows the absorption spectrum obtained upon electrochemical reduction in the presence of protons (in the form of trifluoroacetic acid (TFA)). In contrast to the singly-reduced complex, it does not show an absorption feature at 610 nm. Instead, a very broad and rather flat absorption band above 550 nm and enhanced absorption between 400–530 nm are observed. Additionally, a more drastic decrease of the absorption from 360 to 400 nm takes place in comparison to the non-protonated species. These spectral changes match the ones found for the photoproduct in the photolysis experiment indicating that stabilization of the additional charge by protonation takes place. However, the spectroelectrochemical measurements did not allow to quantify the number of protons (and electrons) involved in the photochemical process. Hence, Figure 8D shows the UV–Vis absorption spectra of the species obtained after successive additions of one equivalent of cobaltocene and one equivalent of TFA to a solution of **RuL1** in CH_3CN, i.e. the singly-reduced (**RuL1**$^-$), singly-reduced singly-protonated (**RuL1H**), doubly-reduced singly-protonated (**RuL1H**$^-$) and doubly-reduced doubly-protonated (**RuL1H$_2$**) derivatives. While cobaltocene (reduction potential of −1.3 V vs Fc^+/Fc in dichloromethane[36]) is not able to reduce **RuL1** twice, charge compensation through protonation significantly alters the

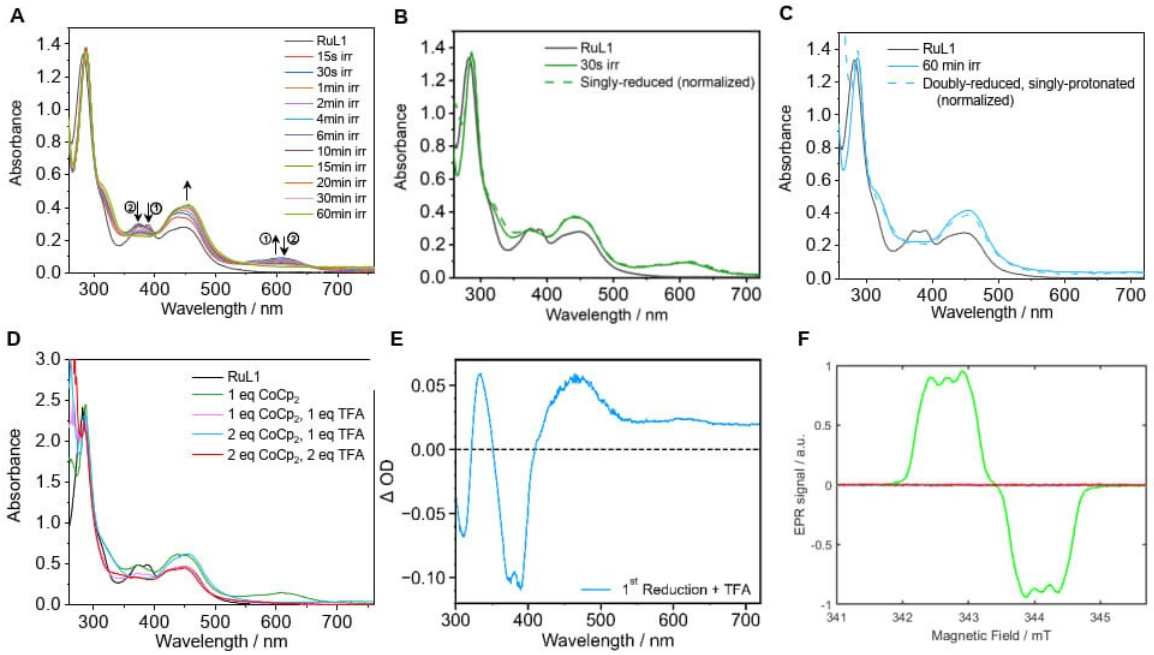

Figure 8. UV–Vis monitoring of the photolysis experiment of **RuL1** (15 μM in CH_3CN) in the presence of triethanolamine (150 mM); B) Comparison of the spectra of the photolysis experiment (t = 30 s; plain line) and the singly-reduced species (dashed line); C) Comparison of the spectra of the photolysis experiment (t = 60 min; plain line) and the doubly-reduced singly-protonated species (dashed line). D) UV–Vis absorption spectra of **RuL1** (black; 15 μM in CH_3CN) and its singly-reduced (red), singly reduced singly-protonated (pink), doubly-reduced singly-protonated (blue), doubly-reduced doubly-protonated derivatives (green), generated via successive chemical reduction and protonation steps with cobaltocene and TFA, respectively. E) UV–Vis difference absorption spectrum of **RuL1** in CH_3CN int the presence of TFA recorded at an applied potential corresponding to the first reduction potential. The electrolyte contained 0.1 M $TBAPF_6$ (scan rate 100 $mV \cdot s^{-1}$, glassy carbon working electrode, Pt counter electrode and Ag/AgCl pseudo-reference electrode). F) Corresponding EPR spectra recorded at room temperature (300 μM in CH_3CN).

redox potentials of the complex, allowing to perform a second reduction process as previously reported for related ruthenium complexes performing multiple charge accumulation.[8,12] Of note, a detailed analysis of the spectra shows that the spectrum of the singly-reduced singly-protonated species (**RuL1H**) is very similar to the one fitted for a 1:1 mixture of **RuL1** and the doubly-reduced doubly-protonated (**$RuL1H_2$**) derivative (Figure S12); this indicates a disproportionation reaction upon protonation of the singly-reduced species. Addition of a second equivalent of reductant and TFA then allows to stoichiometrically generate the complex which is doubly-reduced (and doubly-protonated) on the alloxazine-based ligand. To assist with the assignment of the spectra resulting from stoichiometric reduction and protonation, the spectra of all possible protonation/reduction combinations have been simulated by TDDFT (a summary corresponding to Figure 8 can be found in Figure S13). Taking a closer look at the calculated spectrum of **RuL1H** suggests that a strong increase of the band at around 420 nm would be expected upon formation of the singly-reduced, singly-protonated species due to excited states with high oscillator strengths being available in this region. This behavior cannot be seen in the measurements of the species with stoichiometric amounts of cobaltocene and TFA, instead a decrease in absorption is observed, which fits the calculated behavior of **RuL1** and **$RuL1H_2$** much better. The electronic structure of the four derivatives was further investigated by X-band electronic paramagnetic resonance (EPR) spectroscopy (Figure 8F and S14). The singly-reduced species exhibits a very intense EPR signal, characteristic of an organic radical (g = 2.003). Absolute quantification gives a stoichiometric formation of radical species upon reduction. All other conditions (**RuL1H**, **$RuL1H^-$** and **$RuL1H_2$**) do not produce any EPR signal, indicating that these complexes are formed in a diamagnetic state; this observation for the singly-reduced singly-protonated derivative further supports the disproportionation process. Upon close inspection, the EPR signal of the singly-reduced complex exhibits hyperfine coupling splitting. This spectrum can be successfully simulated by a major species (relative intensity 96.4%) with 3 hyperfine couplings originated from 2 nitrogen atoms (spin 1 nucleus, hyperfine coupling constants of 3.6 MHz and 8.9 MHz) and 1 proton (spin $\frac{1}{2}$ nucleus, hyperfine coupling constant of 6.48 MHz), together with a minor featureless species (relative intensity 3.6%) with a single gaussian line shape (see Table S10, Figure S15). Hyperfine values for the main species are compatible with those previously reported for reduced alloxazine-based ligands,[37] further supporting that the reduction process takes place on the alloxazine ligand. Moreover, the experimental hyperfine values measured for the singly-reduced complex have been successfully reproduced by DFT (Table S11).[38] Based on these data, the comparative analysis of the photolysis and chemical reduction/protonation spectra reveals that the photoproduct formed after one hour of

continuous irradiation is the doubly-reduced singly-protonated derivative (see Figure 8C). Whether disproportionation of the singly-reduced singly-protonated intermediate contributes to the formation of this species under photochemical conditions is not clear at that stage as it might strongly depend on the kinetics of the different processes at work. Of note, while the light-driven generation of the singly-reduced complex is extremely fast, the second stage of the photochemical reaction involving protonation is much slower (one hour), especially when compared with our previously-studied ruthenium complexes based on π-extended aromatic ligands, for which the doubly-reduced doubly-protonated derivatives were formed within 10 minutes under very similar irradiation conditions.[11,12] This underlines that shifting the acid-base equilibria in favor of the protonation of the reduced compound is more difficult with **RuL1**.

Conclusions

This contribution investigated the photophysical properties of the ruthenium complex **RuL1**, featuring a bioinspired alloxazine-based diimine ligand, and its ability to undergo light-driven charge accumulation. We could show that its long-lived excited state is a ^{3}MLCT state in which the charge is localized on the alloxazine-containing ligand. Hence, the electronic structure of this excited state is already similar to the singly-reduced species, a key intermediate in the photochemical reaction. In this singly-reduced species the additional charge is also localized on the alloxazine-based ligand as revealed by rR spectroscopy, EPR and TDDFT. Furthermore, the doubly-reduced derivative of **RuL1** was successfully generated during a photolysis experiment using TEOA as sacrificial electron donor. It was confirmed with the help of redox titrations that protonation is coupled to the photochemical reduction process of **RuL1**. Based on its photophysical properties and the ability to accumulate multiple electrons **RuL1** is a suitable candidate for application in light-driven multielectronic catalysis.

Experimental Section

The ligand **L1** and the complex **RuL1** were prepared according to a previously reported procedure.[18]

All spectroscopic experiments, i. e., steady-state absorption, emission and resonance Raman spectroscopy as well as femtosecond time-resolved transient absorption measurements were performed at room temperature.

For steady-state spectroscopic measurements, the compounds **L1** and **RuL1** were dissolved in DMSO (Roth, ROTIDRY, $\geq$99.5 %, $\leq$200 ppm H_2O) or CH_3CN (Fisher Chemical, $\geq$99.9 %, HPLC gradient grade). UV–Vis absorption spectra were collected on a JASCO V-780 spectrophotometer using a scan rate of 400 nm/min. The emission spectra were recorded using a FLS980 fluorescence spectrometer from Edinburgh Instruments Ltd.

UV–Vis SEC was performed using a three-electrode setup comprising a thinlayer spectroelectrochemical cell with a pathlength of 1 or 2 mm (AdValue Technology, USA), a Pt counter electrode, an Ag/AgCl pseudo-reference electrode and a glassy carbon working electrode. A computer-controlled VersaSTAT 3 (Princeton Applied Research) potentiostat was used to perform cyclic voltammetry and chronoamperometric measurements. Recording of UV–Vis spectra was started shortly before applying the respective reduction potential to monitor the accompanied spectral changes. UV–Vis spectra were collected in transmission mode by using a product of Avantes Inc., which consists of a single-channel fiber-optic spectrometer (AvaSpec-ULS2048XL) equipped with a deuterium/halogen light source (AvaLight DH-S-BAL). Acetonitrile (Fisher Chemical, $\geq$99.9 %, HPLC gradient grade) was dried over CaH_2 and distilled under nitrogen prior to use. Sample solutions with CH_3CN or DMSO (Roth, ROTIDRY, $\geq$99.5 %, $\leq$200 ppm H_2O) containing 0.1 M tetrabutylammonium hexafluorophosphate ($TBAPF_6$) (Sigma Aldrich, for electrochemical analysis, $\geq$98 %) as electrolyte were prepared inside the glovebox.

Resonance Raman measurements were performed using a 405 nm diode laser (TopMode-405-HP, Toptica, Germany), a 473 nm diode-pumped solid-state laser (HB-Laser, Germany) and a 643 nm diode-pumped solid-state DL laser (CrystaLaser, USA) for excitation. Laser powers between 3 and 10 mW were used. Stability of the samples was confirmed by UV–Vis absorption measurements before and after the rR experiments. The Raman signal was detected by an IsoPlane 160 spectrometer (Princeton Instruments, USA) with an entrance slit width of 50 μm and gratings with 600 or 1200 grooves/mm using a thermoelectrically cooled CCD camera of 1340×100 pixels (PIXIS eXcelon, Princeton Instruments, USA). The recorded resonance Raman spectra were background corrected and the band of CH_3CN at 920 cm^{-1} was used as a reference for normalizing intensities. Characterization of the reduced complex **RuL1**$^-$ was carried out on a chemically reduced sample using $CoCp_2$ as reducing agent.

A custom-built setup, which is described in detail elsewhere,[39] was used to record fs-TA data. The output of an amplified Ti:sapphire laser (Libra, Coherent Inc.) was split into two beams. The pulse-to-pulse repetition rate is 1 kHz and pulses are spectrally centered at 800 nm. One of the beams is directed through a BBO crystal to obtain the pump pulses at 400 nm by second harmonic generation. The polarization of the pump pulses is adjusted to the magic angle of 54.7° by a combination of a Berek compensator and a polarizer. A mechanical chopper reduces the repetition rate to 0.5 kHz. The other output beam of the laser is focused into a CaF_2 plate mounted on a rotating stage to generate the white light supercontinuum which serves as probe pulse. The white light is further split into probe and reference pulse. The probe pulse passes a concave mirror of 500 mm focal length which focuses the pulse onto the sample. The white light pulses are recollimated and spectrally dispersed by a prism and detected by a diode array (Pascher Instruments AB, Sweden). Chirp correction of the recorded spectra is carried out by fitting a polynomial to the appearance of the maximal signal amplitude at pulse overlap which corresponds to the arrival time of the different wavelengths of the probe pulse. The resulting time values are then subtracted from the experimental delay values. The corrected data are globally fitted by a sum of exponentials (sequential model). The amplitudes of the exponential fit correspond to the species-associated spectra (SAS). During the fitting, the pulse overlap region of $\pm$300 fs was excluded to avoid contributions from coherent artifacts.[40,41] The chirp correction as well as the fit of the data were performed using the KiMoPack software.[42]

The fluorescence lifetime of **L1** was recorded by streak camera measurements. A Ti:sapphire laser (Tsunami, Newport Spectra-Physics GmbH) was frequency-doubled to generate the 400 nm excitation pulses. The pulse-to-pulse repetition rate of the laser was set to 4 kHz by a pulse selector (Model 3980, Newport Spectra-

Physics GmbH). The emission was detected using a CHROMEX 250IS spectrograph and a Hamamatsu HPD-TA streak camera. The power of the pump pulse was adjusted to 0.4–0.8 mW, and the optical density (OD) of the sample at the excitation wavelength was approximately 0.07.

For the sub-μs time-resolved emission (ns-Em) measurements, which were used to determine the lifetime of the long-lived excited state, the excitation wavelength was set to 440 nm. This pump pulse was generated by a Nd:YAG Laser (Continuum Surelite, 5 ns pulses with a repetition rate of 10 Hz) using an optic parametric oscillator (Continuum Surelite). The time-resolved emission from the sample was recorded with a spectrometer (Acton Princeton Instrument 2300) using a photomultiplier (Hamamatsu R928) and was processed (Pascher Instruments AB). The emission was detected at single wavelengths between 540 and 800 nm in steps of 10 nm.

For chemical reduction with cobaltocene, all the experiments were realized in a nitrogen-filled glovebox. All volume measurements and dilutions were done using micropipettes. UV–Vis absorption spectra were recorded on a Cary 60 UV–Vis (Agilent Technologies) spectrophotometer, equipped with optical fibers. All spectra were zeroed at 600 nm and corrected for increasing volume. The concentration of cobaltocene ($CoCp_2$) solution used for the titration was determined by adding 2 μL aliquots of $CoCp_2$ solution to 3.0 mL of acetonitrile. The concentration was determined by measuring the change in absorbance at 327 nm between successive additions of $CoCp_2$ using the known extinction coefficient for $CoCp_2$ in ethanol of 7420 $L\,mol^{-1}\,cm^{-1}$.[43] Using the calculated concentration of 11.25 mM, it was determined that the first ~0.2 eq of $CoCp_2$ added to the dry degassed acetonitrile solution were used to quench residual oxygen.[7] To perform the chemical reduction titration of **RuL1**, aliquots of the $CoCp_2$ solution (11.25 mM) were then added to a 3 mL solution of **RuL1** (15 μM) in dry degassed acetonitrile and after each addition, the UV–Vis absorption spectrum was recorded.

For the samples characterized by EPR spectroscopy, a final concentration of **RuL1** of 300 μM was used and the UV–Vis absorption spectra were recorded in a 2 mm cuvette. The solution was then transferred inside the glovebox into a specific (home-made) flat cell fitted with Young valves.

Sample preparation and photolysis experiments were carried out in an argon-filled glovebox under low-light conditions. To prepare the photolysis solution, 60 μL of triethanolamine was dissolved in 2.9 mL of dry degassed acetonitrile. To this was added 30 μL of **RuL1** stock solution (1.5 mM) to a final concentration of 15 μM **RuL1** in the photolysis solution. The solution was irradiated using a 300 W ozone-free xenon arc lamp (Newport Ltd.; operated at 280 W) equipped with a 400 nm UV cut-off filter. UV–Vis spectral changes were monitored using a UV–Vis spectrometer after closing the irradiation shutter.

EPR spectra were recorded with a Bruker EMX spectrometer operating at X-band frequency (around 9.53 GHz) with an ER 4104OR Bruker cavity at room temperature. The modulation amplitude was set to 0.5 gauss and the microwave power to 2 mW. For absolute quantification, **RuL1** spectra and reference sample spectra were acquired on the same spectrometer with the same cavity and identical parameters. In each case, the spin number was determined after baseline correction by double integration of the signal. The reference sample was a nitroxide (TEMPO) solution in acetonitrile.

DFT calculations of the ^{14}N and ^{1}H hyperfine coupling constants were performed for the isolated alloxazine ligand **L1** (to be compared to the experimental and DFT values published for the identical PPTD ligand)[37] as well as for the corresponding ruthenium tris-diimine complex **RuL1** with the ADF code[44] using triple-zeta basis sets (no frozen core) and ADF grid precision 6 throughout, combined with several exchange-corrrelation (XC) potentials: i) the Generalized Gradient Approximation (GGA) VBP exchange-correlation (XC) potential [VWN + BP: Vosko, Wilk & Nusair[45] + corrective terms by Becke[46] for the exchange, and Perdew[47] for the correlation]; ii) B3LYP;[48] iii) LB94;[49] iv) OLYP;[50] v) PBE[51] (see Table S11). The geometries have been optimized for the same potentials with the exception of LB94 (not suitable for geometry-optimization) for which the VBP structure has been used instead.

All computational results were obtained by the means of the Gaussian16 software.[52] Additionally, excited state optimizations, were carried out using the external optimizer *pysisyphus* (0.8.0a) in tandem with Gaussian16.[23,52]

Calculations employing density functional theory (DFT) used the B3LYP[53,54] exchange-correlation functional together with the dev2SVP[55,56] basis set and GD3BJ[57] dispersion correction. To address implicit solvent effects, the Solvation Model Density (SMD)[58] variant of the polarizable continuum model (PCM) was used.[58,59] Singlet species were treated using restricted (TD)DFT, whereas doublet and triplet species were treated using unrestricted (TD)DFT, if not mentioned otherwise. Further details with respect to the computational setup are available in the Supporting Information.

Supporting Information

The authors have cited additional references within the Supporting Information.[57,60–63]

Acknowledgements

This work was supported by the French National Research Agency (Labex ARCANE, CBH-EUR-GS, ANR-17-EURE-0003; PhotoAcc project, ANR-19-CE05-0044-01) as well as the German Research Foundation (DFG) within the PhotoAcc project (431449684). Furthermore, SK and BDI are grateful for support within the CRC/TRR 234 CataLight (364549901; A1 and A4). Quantum chemical simulations were performed at the Rechenzentrum of the Friedrich Schiller University Jena and DFT calculations of hyperfine coupling constants (Table S10) have been performed on a local 24-core workstation at Grenoble. Open Access funding enabled and organized by Projekt DEAL.

Conflict of Interests

The authors declare no conflict of interest.

Data Availability Statement

The data that support the findings of this study are available from the corresponding author upon reasonable request.

Keywords: Artificial Photosynthesis · Multielectron Storage · Ruthenium Photosensitizer · Computational Chemistry · Time-Resolved Spectroscopy

[1] L. Hammarström, *Acc. Chem. Res.* **2015**, *48*, 840–850.
[2] T. H. Bürgin, O. S. Wenger, *Energy Fuels* **2021**, *35*, 18848–18856.
[3] Y. Pellegrin, F. Odobel, *Coord. Chem. Rev.* **2011**, *255*, 2578–2593.
[4] D. R. Whang, D. H. Apaydin, *ChemPhotoChem* **2018**, *2*, 148–160.
[5] M. P. O'Neil, M. P. Niemczyk, W. A. Svec, D. Gosztola, G. L. Gaines, M. R. Wasielewski, *Science* **1992**, *257*, 63–65.
[6] R. Konduri, H. Ye, F. M. MacDonnell, S. Serroni, S. Campagna, K. Rajeshwar, *Angew. Chem.* **2002**, *114*, 3317–3319.
[7] S. Singh, N. R. De Tacconi, N. R. G. Diaz, R. O. Lezna, J. Muñoz Zuñiga, K. Abayan, F. M. MacDonnell, *Inorg. Chem.* **2011**, *50*, 9318–9328.
[8] J. M. Aslan, D. J. Boston, F. M. MacDonnell, *Chem. Eur. J.* **2015**, *21*, 17314–17323.
[9] L. Zedler, S. Kupfer, I. R. De Moraes, M. Wächtler, R. Beckert, M. Schmitt, J. Popp, S. Rau, B. Dietzek, *Chem. Eur. J.* **2014**, *20*, 3793–3799.
[10] S. Mendes Marinho, M. Ha-Thi, V. Pham, A. Quaranta, T. Pino, C. Lefumeux, T. Chamaillé, W. Leibl, A. Aukauloo, *Angew. Chem. Int. Ed.* **2017**, *56*, 15936–15940.
[11] J.-F. Lefebvre, J. Schindler, P. Traber, Y. Zhang, S. Kupfer, S. Gräfe, I. Baussanne, M. Demeunynck, J.-M. Mouesca, S. Gambarelli, V. Artero, B. Dietzek, M. Chavarot-Kerlidou, *Chem. Sci.* **2018**, *9*, 4152–4159.
[12] N. M. Randell, J. Rendon, M. Demeunynck, P. Bayle, S. Gambarelli, V. Artero, J. Mouesca, M. Chavarot-Kerlidou, *Chem. Eur. J.* **2019**, *25*, 13911–13920.
[13] R. Foja, A. Walter, C. Jandl, E. Thyrhaug, J. Hauer, G. Storch, *J. Am. Chem. Soc.* **2022**, *144*, 4721–4726.
[14] A. Walter, W. Eisenreich, G. Storch, *Angew. Chem.* **2023**, *135*, e202310634.
[15] T. Hering, B. Mühldorf, R. Wolf, B. König, *Angew. Chem. Int. Ed.* **2016**, *55*, 5342–5345.
[16] W. Olaprath, M. E. McGuire, *Inorg. Chim. Acta* **2012**, *383*, 312–315.
[17] S. Miyazaki, K. Ohkubo, T. Kojima, S. Fukuzumi, *Angew. Chem. Int. Ed.* **2007**, *46*, 905–908.
[18] K. J. Black, H. Huang, S. High, L. Starks, M. Olson, M. E. McGuire, *Inorg. Chem.* **1993**, *32*, 5591–5596.
[19] H. Guo, C. Dang, J. Zhao, B. Dick, *Inorg. Chem.* **2019**, *58*, 8486–8493.
[20] H. Guo, L. Zhu, C. Dang, J. Zhao, B. Dick, *Phys. Chem. Chem. Phys.* **2018**, *20*, 17504–17516.
[21] M. K. Brennaman, T. J. Meyer, J. M. Papanikolas, *J. Phys. Chem. A* **2004**, *108*, 9938–9944.
[22] A. E. Friedman, J. C. Chambron, J. P. Sauvage, N. J. Turro, J. K. Barton, *J. Am. Chem. Soc.* **1990**, *112*, 4960–4962.
[23] J. Steinmetzer, S. Kupfer, S. Gräfe, *Int. J. Quantum Chem.* **2021**, *121*, e26390.
[24] M. Wächtler, J. Guthmuller, L. González, B. Dietzek, *Coord. Chem. Rev.* **2012**, *256*, 1479–1508.
[25] E. Sikorska, M. Sikorski, R. P. Steer, F. Wilkinson, D. R. Worrall, *J. Chem. Soc. Faraday Trans.* **1998**, *94*, 2347–2353.
[26] M. L. Horng, J. A. Gardecki, A. Papazyan, M. Maroncelli, *J. Phys. Chem.* **1995**, *99*, 17311–17337.
[27] M. Gil, Y. Wang, A. Douhal, *J. Photochem. Photobiol. Chem.* **2012**, *234*, 146–155.
[28] Y. Zhang, L. Zedler, M. Karnahl, B. Dietzek, *Phys. Chem. Chem. Phys.* **2019**, *21*, 10716–10725.
[29] N. H. Damrauer, G. Cerullo, A. Yeh, T. R. Boussie, C. V. Shank, J. K. McCusker, *Science* **1997**, *275*, 54–57.
[30] G. B. Shaw, D. J. Styers-Barnett, E. Z. Gannon, J. C. Granger, J. M. Papanikolas, *J. Phys. Chem. A* **2004**, *108*, 4998–5006.
[31] S. Záliš, C. Consani, A. E. Nahhas, A. Cannizzo, M. Chergui, F. Hartl, A. Vlček, *Inorg. Chim. Acta* **2011**, *374*, 578–585.
[32] L. Zedler, P. Wintergerst, A. K. Mengele, C. Müller, C. Li, B. Dietzek-Ivanšić, S. Rau, *Nat. Commun.* **2022**, *13*, 2538.
[33] A. M. Brown, C. E. McCusker, J. K. McCusker, *Dalton Trans.* **2014**, *43*, 17635–17646.
[34] B. Maity, A. Chatterjee, D. Seth, *RSC Adv.* **2015**, *5*, 3814–3824.
[35] Y. Pellegrin, F. Odobel, *Comptes Rendus Chim.* **2017**, *20*, 283–295.
[36] N. G. Connelly, W. E. Geiger, *Chem. Rev.* **1996**, *96*, 877–910.
[37] E. Norambuena, C. Olea-Azar, Á. Delgadillo, M. Barrera, B. Loeb, *Chem. Phys.* **2009**, *359*, 92–100.
[38] J. Casas, D. Pianca, N. Le Breton, A. Jouaiti, C. Gourlaouen, M. Desage-El Murr, S. Le Vot, S. Choua, S. Ferlay, *Inorg. Chem.* **2024**, *63*, 4802–4806.
[39] R. Siebert, D. Akimov, M. Schmitt, A. Winter, U. S. Schubert, B. Dietzek, J. Popp, *ChemPhysChem* **2009**, *10*, 910–919.
[40] B. Dietzek, T. Pascher, V. Sundström, A. Yartsev, *Laser Phys. Lett.* **2007**, *4*, 38–43.
[41] A. L. Dobryakov, S. A. Kovalenko, N. P. Ernsting, *J. Chem. Phys.* **2005**, *123*, 044502.
[42] C. Müller, T. Pascher, A. Eriksson, P. Chabera, J. Uhlig, *J. Phys. Chem. A* **2022**, *126*, 4087–4099.
[43] A. Jaworska-Augustyniak, J. Wojtczak, *Monatshefte Für Chem.* **1979**, *110*, 1113–1121.
[44] G. Te Velde, E. J. Baerends, *J. Comput. Phys.* **1992**, *99*, 84–98.
[45] S. H. Vosko, L. Wilk, M. Nusair, *Can. J. Phys.* **1980**, *58*, 1200–1211.
[46] A. D. Becke, *Phys. Rev. A* **1988**, *38*, 3098–3100.
[47] J. P. Perdew, *Phys. Rev. B* **1986**, *33*, 8822–8824.
[48] P. J. Stephens, F. J. Devlin, C. F. Chabalowski, M. J. Frisch, *J. Phys. Chem.* **1994**, *98*, 11623–11627.
[49] R. Van Leeuwen, E. J. Baerends, *Phys. Rev. A* **1994**, *49*, 2421–2431.
[50] N. C. Handy, A. J. Cohen, *Mol. Phys.* **2001**, *99*, 403–412.
[51] J. P. Perdew, K. Burke, M. Ernzerhof, *Phys. Rev. Lett.* **1996**, *77*, 3865–3868.
[52] G. W. T. M. J. Frisch, H. B. Schlegel, G. E. Scuseria, M. A. Robb, J. R. Cheeseman, G. Scalmani, V. Barone, G. A. Petersson, H. Nakatsuji, X. Li, M. Caricato, A. V. Marenich, J. Bloino, B. G. Janesko, R. Gomperts, B. Mennucci, H. P. Hratchian, J. V. Ortiz, A. F. Izmaylov, J. L. Sonnenberg, D. Williams-Young, F. Ding, F. Lipparini, F. Egidi, J. Goings, B. Peng, A. Petrone, T. Henderson, D. Ranasinghe, V. G. Zakrzewski, J. Gao, N. Rega, G. Zheng, W. Liang, M. Hada, M. Ehara, K. Toyota, R. Fukuda, J. Hasegawa, M. Ishida, T. Nakajima, Y. Honda, O. Kitao, H. Nakai, T. Vreven, K. Throssell, J. A. Montgomery, Jr., J. E. Peralta, F. Ogliaro, M. J. Bearpark, J. J. Heyd, E. N. Brothers, K. N. Kudin, V. N. Staroverov, T. A. Keith, R. Kobayashi, J. Normand, K. Raghavachari, A. P. Rendell, J. C. Burant, S. S. Iyengar, J. Tomasi, M. Cossi, J. M. Millam, M. Klene, C. Adamo, R. Cammi, J. W. Ochterski, R. L. Martin, K. Morokuma, O. Farkas, J. B. Foresman, D. J. Fox, *Gaussian 16, Rev. B.01; Gaussian Inc.: Wallingford, CT* **2016**
[53] A. D. Becke, *J. Chem. Phys.* **1992**, *96*, 2155–2160.
[54] C. Lee, W. Yang, R. G. Parr, *Phys. Rev. B* **1988**, *37*, 785–789.
[55] F. Weigend, R. Ahlrichs, *Phys. Chem. Chem. Phys.* **2005**, *7*, 3297.
[56] F. Weigend, *Phys. Chem. Chem. Phys.* **2006**, *8*, 1057.
[57] S. Grimme, S. Ehrlich, L. Goerigk, *J. Comput. Chem.* **2011**, *32*, 1456–1465.
[58] A. V. Marenich, C. J. Cramer, D. G. Truhlar, *J. Phys. Chem. B* **2009**, *113*, 6378–6396.
[59] B. Mennucci, C. Cappelli, C. A. Guido, R. Cammi, J. Tomasi, *J. Phys. Chem. A* **2009**, *113*, 3009–3020.
[60] J. Guthmuller, L. González, *Phys. Chem. Chem. Phys.* **2010**, *12*, 14812.
[61] A. D. Becke, *J. Chem. Phys.* **1993**, *98*, 5648–5652.
[62] J. P. Merrick, D. Moran, L. Radom, *J. Phys. Chem. A* **2007**, *111*, 11683–11700.
[63] J. Guthmuller, *J. Chem. Phys.* **2016**, *144*, 064106.

Manuscript received: May 15, 2024
Revised manuscript received: August 5, 2024
Accepted manuscript online: August 15, 2024
Version of record online: ■■, ■■

RESEARCH ARTICLE

The ability of an alloxazine-containing ruthenium complex to accumulate electrons upon illumination in the presence of a sacrificial electron donor is demonstrated. Moreover, its photophysical properties are studied by absorption, emission, resonance Raman, transient absorption spectroscopy and quantum chemical simulations.

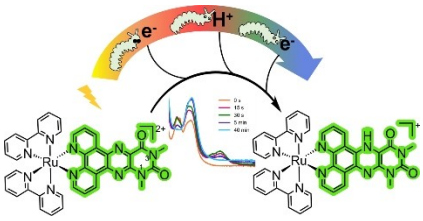

N. Hagmeyer, A. Schwab, Dr. N. Mroweh, Dr. C. McManus, Dr. M. Varghese, Dr. J.-M. Mouesca, Dr. S. Gambarelli, Dr. S. Kupfer, Dr. M. Chavarot-Kerlidou*, Prof. Dr. B. Dietzek-Ivanšić**

1 – 11

Spectroscopic Investigation of a Ruthenium Tris-Diimine Complex Featuring a Bioinspired Alloxazine Ligand